ARMY RESEARCH LABORATORY

Numerical Simulation of Sabot Discard Aerodynamics

Michael J. Nusca

ARL-TR-204 September 1993

NOTICES

Destroy this report when it is no longer needed. DO NOT return it to the originator.

Additional copies of this report may be obtained from the National Technical Information Service, U.S. Department of Commerce, 5285 Port Royal Road, Springfield, VA 22161.

The findings of this report are not to be construed as an official Department of the Army position, unless so designated by other authorized documents.

The use of trade names or manufacturers' names in this report does not constitute indorsement of any commercial product.

REPORT DOCUMENTATION PAGE

Form Approved
OMB No. 0704-0188

1. AGENCY USE ONLY *(Leave blank)*	2. REPORT DATE	3. REPORT TYPE AND DATES COVERED
	September 1993	Final Jan 1992 - Dec 1992

4. TITLE AND SUBTITLE

Numerical Simulation of Sabot Discard Aerodynamics

5. FUNDING NUMBERS

PR: 1L161102AH43

6. AUTHOR(S)

Michael J. Nusca

7. PERFORMING ORGANIZATION NAME(S) AND ADDRESS(ES)

U.S. Army Research Laboratory
ATTN: AMSRL-WT-PE
Aberdeen Proving Ground, MD 21005-5066

8. PERFORMING ORGANIZATION REPORT NUMBER

9. SPONSORING/MONITORING AGENCY NAMES(S) AND ADDRESS(ES)

US Army Research Laboratory
ATTN: AMSRL-OP-CI-B (Tech Lib)
Aberdeen Proving Ground, MD 21005-5066

10.SPONSORING/MONITORING AGENCY REPORT NUMBER

ARL-TR-204

11. SUPPLEMENTARY NOTES

12a. DISTRIBUTION/AVAILABILITY STATEMENT

Approved for public release; distribution is unlimited.

12b. DISTRIBUTION CODE

13. ABSTRACT *(Maximum 200 words)*

Computational fluid dynamics (CFD) solutions of the three-dimensional Navier-Stokes equations have been applied to sabot discard aerodynamics for gun-launched, saboted, armor-piercing projectiles. The portion of the launch cycle that involves strong aerodynamic interference between the projectile and discarding sabot (carrier) components has been investigated. Three sabot components were located symmetrically at various positions near the projectile and at angle of attack. The complex system of shock/boundary-layer interactions between multiple bodies (projectile and sabots), during the discard sequence, has been numerically simulated. Computed and measured surface pressures compare favorably for Mach number 4.5 and Reynolds number six million per meter. Comparison of symmetric sabot discard trajectories predicted using CFD and the AVCO sabot design code are shown.

14. SUBJECT TERMS	15. NUMBER OF PAGES
Navier Stokes equations, sabot, launch dynamics, aerodynamics, kinetic energy projectiles	39
	16. PRICE CODE

17. SECURITY CLASSIFICATION OF REPORT	18. SECURITY CLASSIFICATION OF THIS PAGE	19. SECURITY CLASSIFICATION OF ABSTRACT	20. LIMITATION OF ABSTRACT
UNCLASSIFIED	UNCLASSIFIED	UNCLASSIFIED	SAR

INTENTIONALLY LEFT BLANK

TABLE OF CONTENTS

INTENTIONALLY LEFT BLANK

LIST OF FIGURES

Acknowledgment

The author is indebted to Dr. E. Schmidt, Propulsion and Flight Division, Aerodynamics Branch, who supported this work, and to Mr. D. Savick for reviews and information regarding the AVCO code.

INTENTIONALLY LEFT BLANK

1. INTRODUCTION

Currently, the most widely used design for kinetic energy, antitank applications is the gun-launched, fin-stabilized, long-rod projectile. The cross-sectional diameter of the rod is much smaller than the diameter of the gun bore. Fins span the area between the rod and the gun tube. Therefore, a sabot (or carrier) is required to provide obturation for the projectile and to minimize its in-bore balloting. Once free of the gun tube, the sabot must be discarded in order to permit unconstrained, low-drag flight to the target. The sabot is divided into three or four components along axial planes. For smooth bore gun tubes, these components separate from the projectile under the action of elastic and aerodynamic loads. Figures 1 and 2 show a photograph and shadowgraph of typical sabot discard during free flight.

It has been demonstrated (Schmidt et.al. 1978) that aerodynamic interference generated by the sabot components can be a significant source of projectile launch disturbance leading to unacceptable loss of accuracy at the target. Perturbations to the projectile's trajectory are magnified by geometric asymmetry in the discard pattern and by extended periods during launch when the sabot components are in close proximity to the projectile. A detailed understanding of the three-dimensional shock/boundary-layer interference flowfield between the sabot and the projectile (see Figure 2) is not available.

An extensive experimental program to investigate the aerodynamics of sabot discard has been conducted (Schmidt 1981). During these tests, a projectile and three sabot components were sting-mounted in the NASA Langley Unitary Plan wind tunnel facility 4 x 4 ft test section. The model configuration included a stationary cone-cylinder projectile (without fins) at zero angle-of-attack and three 120° included-angle sabot components located symmetrically around the projectile. Figure 3 shows a schematic (cross-section) of the wind tunnel model (one sabot shown). The cylinder section of the projectile was 50.8mm in diameter; the projectile had a length-to-diameter ratio of 10.5 and a 30° included-angle conical nose. Fifty static pressure taps were positioned on the surface between the 120° planes of symmetry, with four taps on the conical section. The sabot had cylindrical inner and outer surfaces of radii 25.4 and 76.2mm, respectively, with the a leading edge chamfer of 40°. Fifty static pressure taps were located on the inner and outer surfaces. The test Mach number and Reynolds number were 4.5 and 6.6 million per meter, respectively. A typical flight Reynolds number of 89 million per meter could not be reproduced in the tunnel. Test results showed regions of shock/boundary-layer interaction, separated flow and other viscous phenomena which are sensitive to the Reynolds number.

Initial analytical work for steady state sabot discard aerodynamics relied on the Newtonian flow approximation and empirical aerodynamic interaction analyses, for example, the AVCO code (Crimi et.al. 1977, Seigelman et.al. 1983). Consideration was limited to a general sabot configuration, bound radially by two cylindrical surfaces and axially by two conical surfaces. These assumptions make discard computations tractable and in some cases represent accurate approximations. However, it is apparent that the multiple shock/expansion interaction flowfield between the projectile and sabot petals is an essential part of the analysis. The initial version of the AVCO code (Crimi et.al. 1977) evaluated the aerodynamic loadings on the sabot segments using Newtonian theory and a subsonic/supersonic inlet model; pressure forces on each surface of the segments, including sabot sides, were obtained separately and summed to provide results for total force and moments (excluding shear stress components). The code assumed that the aerodynamic coefficients for the projectile were known. Although the sabot separation process is initially dominated by aerodynamic interaction, the code assumed one-dimensional flow between the bodies. Recent versions (Seigelman et.al. 1983) include an integrated flow element approach utilizing local shock/expansion procedures based on sabot surface pressures measured during wind tunnel tests (Schmidt 1981). These test data are used to determine pressure levels on certain sabot locations with linear variations assumed between these points. As a result, the code includes the effects of pressure pulses on the bodies caused by impinging and reflecting shock waves. To calculate the initial sabot lift-off aerodynamic forces and then again when the sabot petals are not in close proximity to the projectile, Newtonian flow theory is used. In some cases, however, these code improvements produced overestimates of the discard process in contrast to initial code predictions.

This report describes computational fluid dynamics (CFD) solutions applied to the three-dimensional (3D) Navier-Stokes equations for symmetric sabot discard. During symmetric discard multiple sabot components are assumed to follow identical trajectories away from the projectile, and the projectile is assumed to be at zero angle-of-attack. As shown in Figure 4, the computational domain can therefore be limited to a smaller portion of the entire flowfield around the configuration; this reduces computational grid size, computer memory, and computer run time. For three sabot components this domain spans a 60° sector from sabot midplane to symmetry plane between neighboring sabot components. For asymmetric discard the computational domain would be greatly expanded (i.e. a full 360° sector) with a corresponding increase in computer requirements. The portion of the launch cycle that involves strong aerodynamic interference between the projectile and the sabot components is examined. Thus, simulations are performed for small vertical separation of the sabot from the projectile surface, $\Delta y/D \leq 1$ (D = projectile rod diameter = 1 cal. or 50.8mm in Figure 3) and sabot angle of attack $\alpha \leq 10^{\circ}$. Previous work described code validation with

wind tunnel results (Nusca Aug. 1990, Oct. 1990). A four-stage sabot discard sequence was numerically simulated for the wind tunnel model configuration (Nusca Apr. 1991, Jul. 1991). In this report these simulations have been extended to ten stages with resultant aerodynamic forces and moments computed from the flowfield. The symmetric sabot discard trajectory is then simulated and compared to results obtained using the AVCO code. This quasi-steady, programmed simulation ignores the flow time dynamics and does not link the aerodynamic forces to the sabot motion. However, such a simulation serves as a prelude to computations that utilize coupling of unsteady aerodynamics and rigid-body motion. The flowfield for a M865 projectile/sabot is also simulated.

2. COMPUTATIONAL APPROACH

CFD can be used to simulate the compressible flowfield around aerodynamic bodies by solving the 3D Reynolds-averaged Navier-Stokes (RANS) equations. The USA-PG3 code was developed by Chakravarthy (1985, 1988). The RANS equations are written using a perfect gas assumption. Both laminar and turbulent flows can be investigated thus, a turbulence model (Baldwin 1978) is required for closure. In addition, backflow regions can be present thus, a backflow turbulence model (Goldberg 1986) is included. The equations are transformed into the conservation law form and discretized using finite-volume approximations. The USA-PG3 code uses a class of numerical algorithms termed total variational diminishing (TVD). The resulting set of equations is solved using an implicit, factored, time-stepping algorithm. The solution takes place on a computational grid that is generated around the configuration in zones; zonal boundaries are transparent to the flowfield.

2.1 Equations of Motion. The RANS equations for 3D flow are written in the following conservation form. The dependent variables u, v, w, and e are mass-averaged.

$$\frac{\partial W}{\partial t} + \frac{\partial F}{\partial x} + \frac{\partial G}{\partial y} + \frac{\partial H}{\partial z} = 0 \tag{1}$$

$$W = (\rho \quad \rho u \quad \rho v \quad \rho w \quad \rho e)$$

$$F = \begin{pmatrix} \rho u \\ \rho u^2 - \sigma_{xx} \\ \rho uv - \tau_{xy} \\ \rho uw - \tau_{xz} \\ \rho ue + \dot{q}_x - \sigma_{xx} u - \tau_{xy} v - \tau_{xz} w \end{pmatrix}$$

Arrays G and H are similar in form to array F (see Nusca Oct. 1990). Normal stress (σ), shear stress (τ), heat transfer ($\dot{q}$) and energy (e) are defined elsewhere (Nusca Oct. 1990). The laminar and eddy viscosities, μ and μ_t, are implicitly divided by the reference Reynolds number (Re). The flow medium is assumed to be a perfect gas satisfying the equation of state $p = \rho \Re T$. A power law (Mazor et.al. 1985) is used to relate molecular viscosity, μ, to temperature. The laminar and turbulent Prandtl numbers, Pr and Pr_t, are assumed to be constant with values of 0.72 and 0.9, respectively. The ratio of specific heats, γ, is also assumed constant. Assuming a time-invariant grid and using the transformation of coordinates implied by $\tau = t, \xi = \xi(x, y, z), \eta = \eta(x, y, z)$, and $\zeta = \zeta(x, y, z)$, Equation 1 can be recast into the conservation form where ξ, η, and ζ are the new independent variables, and x_ξ, x_η, x_ζ, y_ξ, y_η, y_ζ, z_ξ, z_η, and z_ζ are the nine transformation coefficients obtained numerically from the mapping procedure. Transformed time is represented by τ.

$$\frac{\partial W}{\partial \tau} + \frac{1}{\text{Area}} [(y_\eta F - x_\eta G)_\xi + (-y_\xi F + x_\xi G)_\eta + G/y - H/y] = 0 \qquad (2)$$

The "Area" in Equation 2 denotes the area of the finite volume cell being considered at the time of discretization of the equations.

The shock/boundary-layer interference flowfield between projectile and sabots can include regions of recirculating flow. To improve the predictive capability of separated flows using RANS codes a new turbulence model has been recently developed by Goldberg (1986). The new model is based on experimental observations of detached flows and allows turbulence due to local shear effects to be taken into account in addition to wall-shear contributions. The velocity scale function, which is normally $y\omega$, is modified as $(y - y_e)\omega$ (for $y \geq y_e$). Here, ω is the magnitude of the local vorticity and y_e is the location away from the wall where the vorticity first diminishes to a small fraction ($\leq 5\%$) of the local maximum magnitude. From this location onward the length scale is given by $y_{\max} - y_e$. The model prescribes turbulence kinetic energy and dissipation analytically within backflows. A formula for the eddy viscosity (μ_t) within backflows is derived and used for the RANS equations when calculations are done inside separation bubbles. Outside of them, another turbulence model (Baldwin et.al. 1978) supplies the values of eddy viscosity.

2.2 Computational Algorithm. The spatial discretization technique for the equations of motion must successfully capture the complex physics of interacting projectile/sabot flowfields. The TVD formulation for the convective terms along with a special treatment of the dissipative terms (Equation 1) provides an appropriate simulation. In recent years, TVD formulations have been constructed for shock-capturing finite-difference methods (Chakravarthy et.al. 1985,1988). Near large gradients in the solution (extrema) TVD algorithms automatically reduce to first-order accurate discretizations locally while away from extrema they

can be constructed to be of higher-order accuracy. This local effect restricts the maximum global accuracy possible for TVD algorithms to third order for steady-state solutions. TVD methods manifest many properties desirable in numerical solution procedures. By design they avoid numerical oscillations and "expansion shocks" while at the same time being of higher-order accuracy. TVD formulations are also based on the principle of discrete or numerical conservation which is the numerical analog of physical conservation of mass, momentum, and energy. Thus, TVD algorithms can "capture" flowfield discontinuities (e.g. shock waves) with high resolution. At a fundamental level they are based on upwind algorithms; therefore, they closely simulate the signal propagation properties of hyperbolic equations. Algorithms based on the TVD formulation are completely defined. In contrast, algorithms based solely on central differences involve global dissipation terms for stability and have one or more coefficients that must be judiciously chosen to achieve desirable results. Any conventional time discretization method suitable for the Navier-Stokes equations can be used together with this space discretization methodology; for example, approximate factorization and relaxation techniques.

2.3 Computational Grid. Numerical simulation of the interacting flowfield about projectile/sabot combinations is complicated by the non-axisymmetric, multiple-wall geometry. The computational domain is divided into zones of simple geometric shape. In each zone an algebraic grid is generated with grid clustering near walls and high flow gradient regions. The computational method is constructed such that each zone is considered an independent module interacting with other zones before or after the information corresponding to each zone is updated one cycle. Zonal boundaries are transparent to the flowfield. A typical 6-zone grid used for computations described in this report is designed as follows (see Figures 5 and 6): grid zone 1 covers the projectile from nose to base, zone 2 covers the area between zone 1 and the inner surface of the sabot, zone 4 covers the area between the outer surface of the sabot and the uppermost extent of the computational domain, zones 5 and 6 cover the projectile and sabot base regions, respectively. Zones 1 thru 6, excluding zone 3, extend from $\phi = 0$ to 60° in the azimuthal direction. Grid zone 3 covers the area between the sabot and the azimuthal extent of the computational domain. The entire 6-zone grid consists of 300,000 nodes and requires 10 million words of memory on a CRAY-2 supercomputer. Converged solutions require about 10 CPU hours.

3. RESULTS

Figure 7 shows the measured (Schmidt 1981) and computed pressure distributions over the projectile and sabot surface in the pitch plane; the pitch plane (see Figure 4) bisects the azimuthal planform of the sabot. Three sabot components are modeled with sabot bases aligned with the projectile base, $\Delta x/D = 0$, projectile surface and sabot inner surface vertically separated by $\Delta y/D = .75$, with the sabots at zero angle-of-attack. Laminar boundary layer modeling was employed; turbulent solutions are described elsewhere (Nusca Aug. 1990, Oct. 1990). Computed pressures on the projectile surface agree favorably with the magnitude and location of a measured pressure peak ($x/D \simeq 4.22$) as well as elevated pressures preceding this peak, $2 \leq x/D \leq 4.22$. The location of this pressure peak corresponds to the termination of a low speed flow region on the projectile. Downstream of the pressure peak the agreement between computation and measurement is also favorable. On the inner surface of the sabot, numerical simulation adequately predicts the pressure level and trend on the sabot slant surface, $2.75 \leq x/D \leq 3.94$. Pressure trends on the rest of the sabot section agree with measurements including a pressure rise at $x/D \simeq 5.5$.

Nusca (1990, 1991) describes further results obtained for the wind tunnel model, summarized here. For cases when the sabot petals are close to the projectile ($\Delta y/D \leq .75$), a low speed ($M \leq 1$) recirculating flow pocket forms between the projectile and the beveled section of the sabot petals. This causes a strong impinging oblique shock on the projectile surface where the pocket forms and a high pressure pulse where the pocket terminates. As the sabot petals discard, a normal shock, formed at the leading edge of the sabot, becomes an oblique shock that intersects the projectile surface in a regular reflection. Inviscid flow simulations require significantly less computer time by excluding the viscous terms in the Navier-Stokes equations. However, the inviscid simulation predicts lower pressures on the projectile and sabot than measured or predicted by laminar and turbulent simulations. Turbulent calculations are similar to laminar for the low Reynolds number wind tunnel data. Comparison of CFD predictions with projectile surface data measured azimuthally about the projectile agree with the trend but not the magnitude of these pressures (in particular the pressure peak, as shown in Figure 7, reduces as measured azimuthally about the body). Azimuthal grid refinement increases the level of agreement. Computations for the 2D/axisymmetric equivalent of three sabot petals (i.e. petals joined into a concentric tube with the projectile centerline) are computationally inexpensive but result in flowfields that are very different from the 3D case.

Figures 8 through 17 show computed laminar, steady-state, pressure contours in the pitch plane for the forward part of the projectile/sabot configuration and ten stages of the

programmed discard sequence. Three horizontal lines extending from $x/D = 0$ to 7.03 are zonal grid boundaries. Large flow gradients (e.g. shock waves) are indicated by clustering of pressure contour lines. Pressure contour levels are the same for Figures 9-17, $1 \leq P/P_\infty \leq 40, \Delta P/P_\infty = .5$; however, for Figure 8, $1 \leq P/P_\infty \leq 10^0, \Delta P/P_\infty = 1$ due to higher stagnation pressures.

The programmed discard sequence shown in Figures 8-17 covers four vertical displacements of the sabot inner surface with respect to the projectile surface ($\Delta y/D$) and six sabot angles of attack (with respect to the projectile). The projectile was assumed to be at zero yaw with respect to the freestream and the Mach number was constant as 4.5. Since the time during which the sabot petals and projectile are in close proximity is usually short (about 2 ms or 1.5 meters from the gun), the assumption of constant Mach number is not unreasonable. This quasi-steady, programmed simulation ignores the flow time dynamics and does not link the aerodynamic forces to the sabot motion. However, such a simulation serves as a prelude to computations that utilize coupling of unsteady aerodynamics and rigid-body motion.

As seen in Figures 8-17, the sabot generates a strong series of shock waves, beginning as a detached nearly-normal shock that intersects the projectile surface as a strong oblique shock, and ending as an attached oblique shock that intersect the projectile surface in a regular reflection. Flow between the sabot inner surface and the projectile surface begins as a choked nearly-uniform high pressure field with transition into reflected shocks (from sabot back to projectile) that become more pronounced. Beginning with Figure 12, a low pressure recirculation bubble develops on the sabot inner surface extending from $x/D = 3.94$ to the next shock impingement on the sabot surface. Combined with the high pressure on the sabot beveled sectic (2.75 $\leq x/D \leq$ 3.94) this low pressure region provides a force couple that promotes sabot discard.

Using the simulated sabot discard sequence described above, the corresponding aerodynamic forces (lift and drag) and pitching moment can be computed. This is accomplished by integrating the sabot surface pressure and shear stress distributions for each stage of the discard sequence. The sabot mass properties are used to compute vertical and horizontal accelerations which are assembled in a table as functions of sabot $\Delta y/D$ and α. A modified point-mass trajectory model is used to compute the sabot center of gravity (CG) location as a function of time using double-interpolation from values in the table. Figure 18 shows a comparison between the sabot CG location (both in the axial and radial directions) computed using the AVCO semi-empirical code and the present simulation using CFD. The present predictions match the AVCO values for early times, but diverge later in the simulated discard event. In the AVCO simulation sabot discard progresses faster than predicted

using the current method. The relatively good agreement for early times in the discard event may be a result of the sabot/projectile interference methods included in the AVCO code. Reasons for discrepancies in the predictions at later times are still under investigation. One possibility is that the Newtonian theory used to predict aerodynamic forces when the sabot is not in close proximity to the projectile, results in lift and drag values that are larger than predicted using CFD. In comparing the AVCO prediction to that using CFD, several points should be noted. Both methods used the same sabot geometry and mass properties, freestream flow conditions and assumed a symmetric discard. Both methods are quasi-steady in nature, using a database of steady aerodynamic force predictions to simulate a dynamic event. However, the source of the aerodynamic data is very different between the codes (see "Introduction" for a discussion of the AVCO code). By virtue of the rapid aerodynamic methods incorporated into the AVCO code, a much larger aerodynamic force and moment database is available. The trajectory time-integration step for the AVCO code was much smaller that that used in the present study.

Figure 19 shows the projectile/sabot configuration of the Army M865 anti-tank round. The configuration has been altered somewhat in order to simplify computational grid generation. These alterations are also illustrated in Figure 19. The sabot was located .75 calibers above the projectile (1 caliber = 38mm) and at zero angle-of-attack. Figure 20 shows the computational grid. A simulated sabot discard sequence like that used for the wind tunnel model is in progress. Figure 21 shows the laminar flow pressure contours for the M865. The Reynolds number for this flow is 6.6 million per meter and the freestream Mach number is 4.5.

4. CONCLUSIONS

CFD solutions of the 3D Navier-Stokes equations have been applied to the aerodynamics of symmetric sabot discard. A steady simulated sabot discard sequence using fixed sabot locations (with respect to the projectile) reveals shock/shock and shock/boundary-layer interactions in the flowfield. The freestream Mach number was 4.5 and laminar boundary layer modeling was employed for Reynolds number 6.6 million per meter. Numerical simulations have also been performed using Reynolds number 89 million per meter and flows with turbulence modeling (Nusca Aug. 1990). The steady-state approach that uses predetermined sabot positions has lead to enhanced understanding of the discard event, serving as a prelude to computations that utilize coupling of unsteady aerodynamics and rigid-body motion. A technique for the integration of surface pressures and shear stress was developed for the wind tunnel model sabot.

Numerical mesh generation for the solution of complex flowfields about realistic projectile/sabot configurations may be greatly simplified by the use of unstructured (i.e. finite-element like) grids. Figure 22 shows the planar view (i.e. slice through the pitch plane of the projectile/sabot) of a typical unstructured grid for the Army M829 sabot. Solution of the Euler equations on unstructured grids is being accomplished by Chakravarthy (1991). Work on unstructured grids and moving grid zones will eventually lead to a more realistic simulation of the discard event.

INTENTIONALLY LEFT BLANK

Figure 1. Photograph of typical kinetic energy long-rod projectile in free flight during three-petal sabot discard.

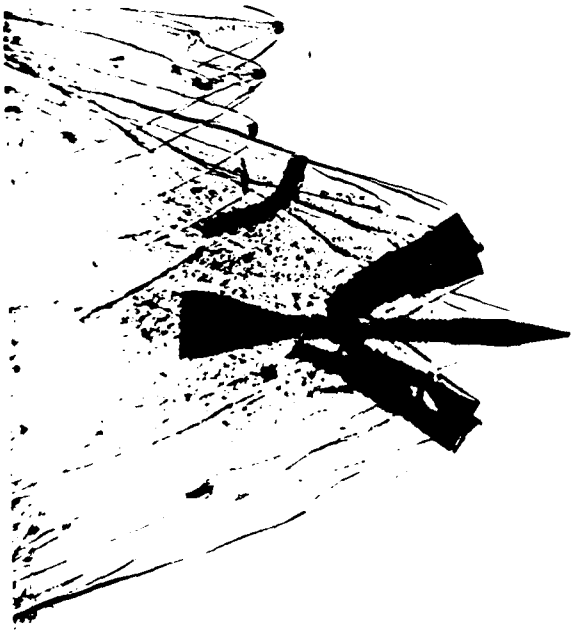

Figure 2. Shadowgraph of typical kinetic energy long-rod projectile in free flight during four-petal sabot discard.

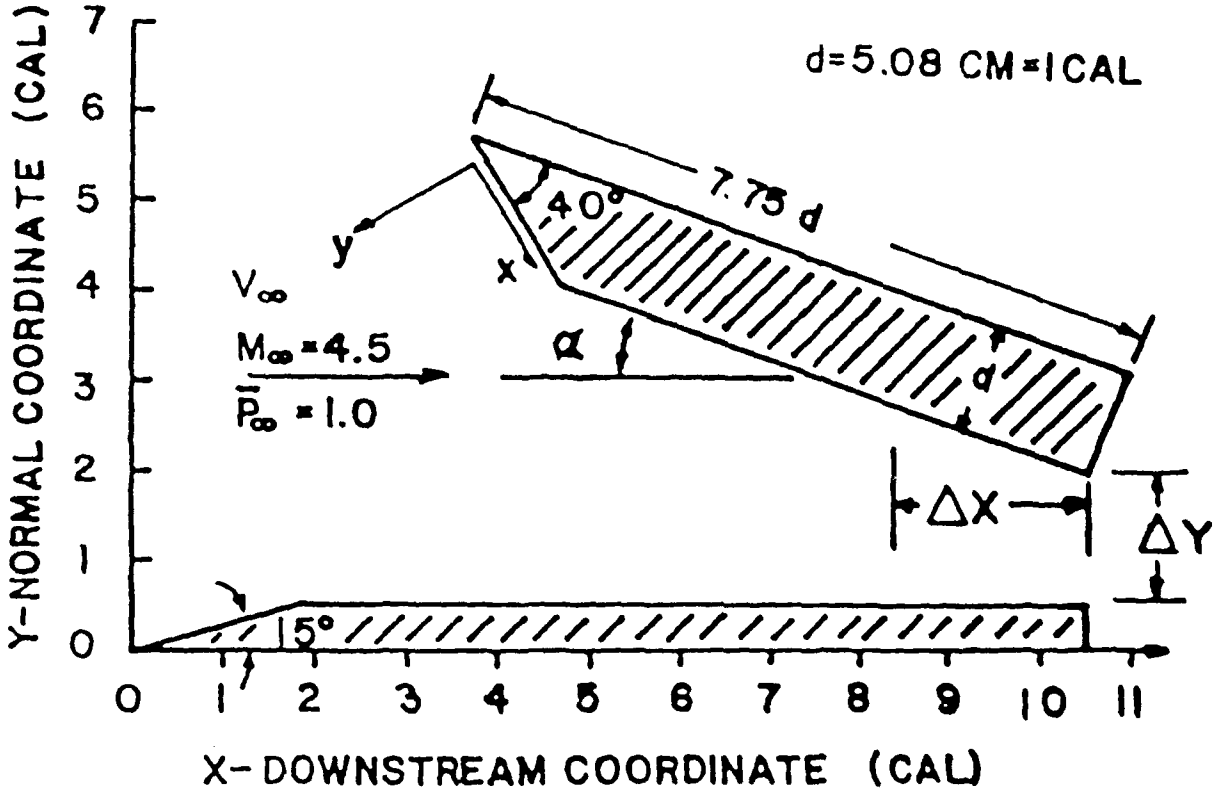

Figure 3. Schematic of wind tunnel model in the pitch plane ($\phi = 0, 180°$).

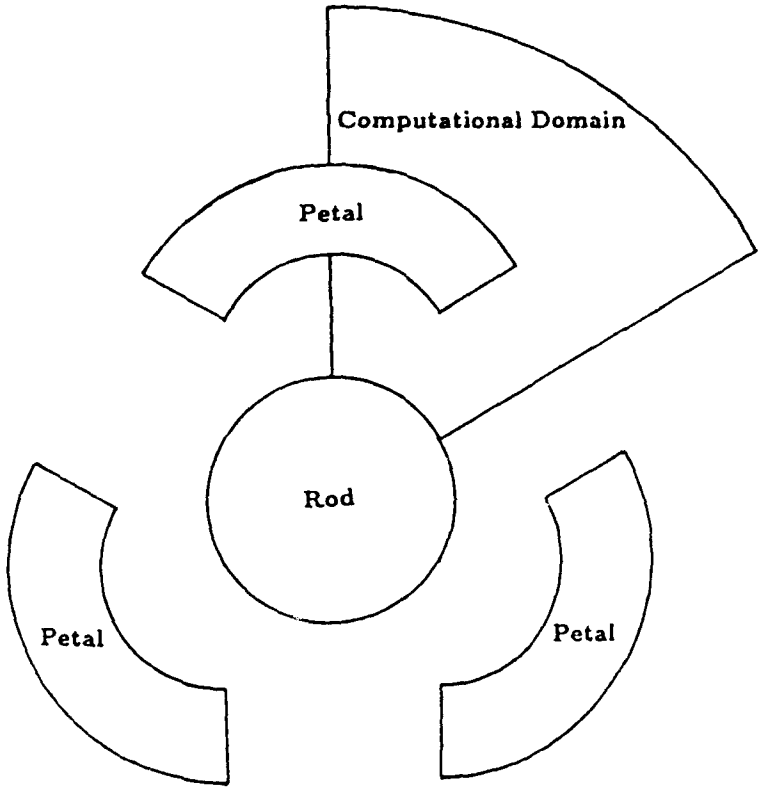

Figure 4. Schematic of symmetric sabot discard (rear-view) showing computational domain.

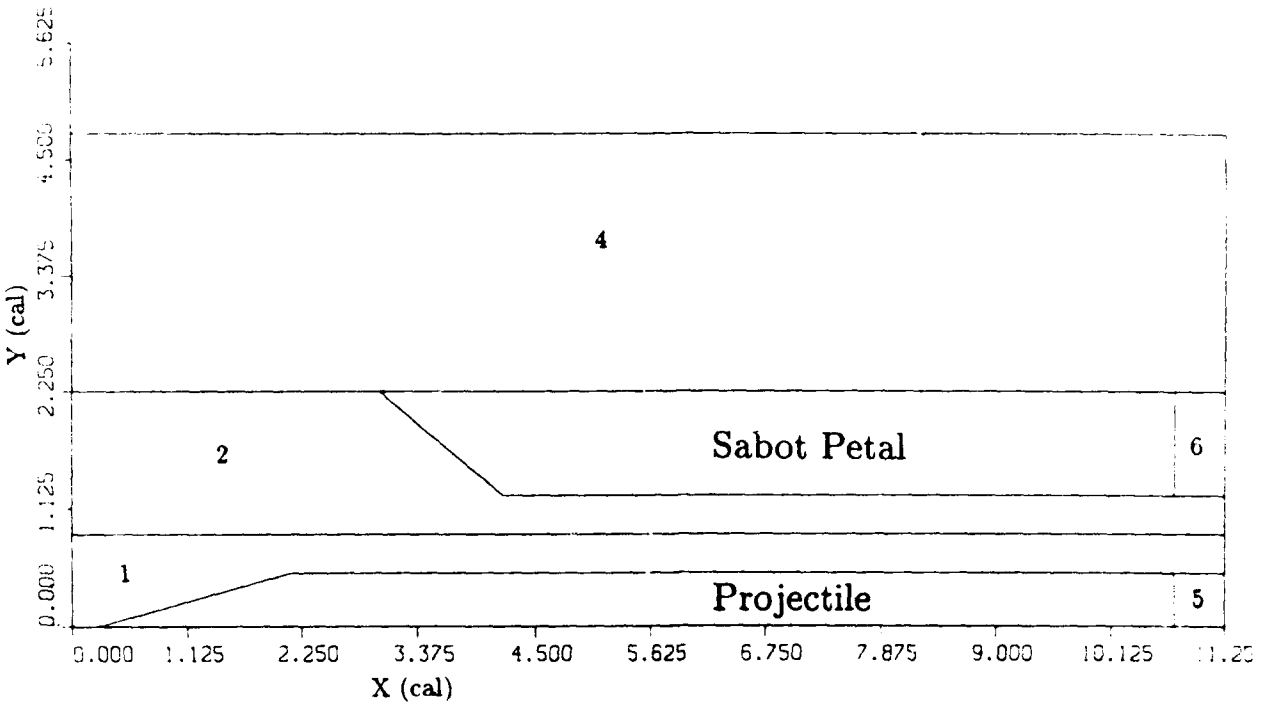

Figure 5. Zone designations for projectile/sabot configuration in the pitch plane

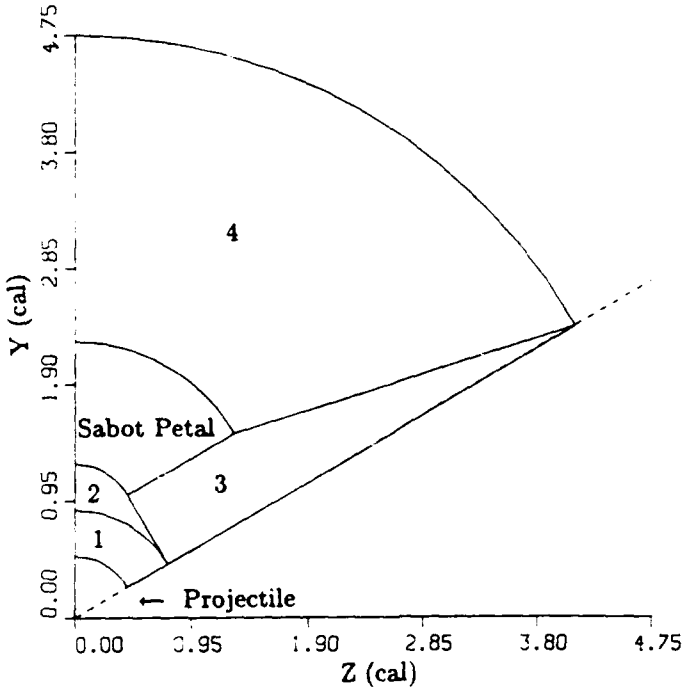

Figure 6. Zone designations for projectile/sabot configuration in an axial plane

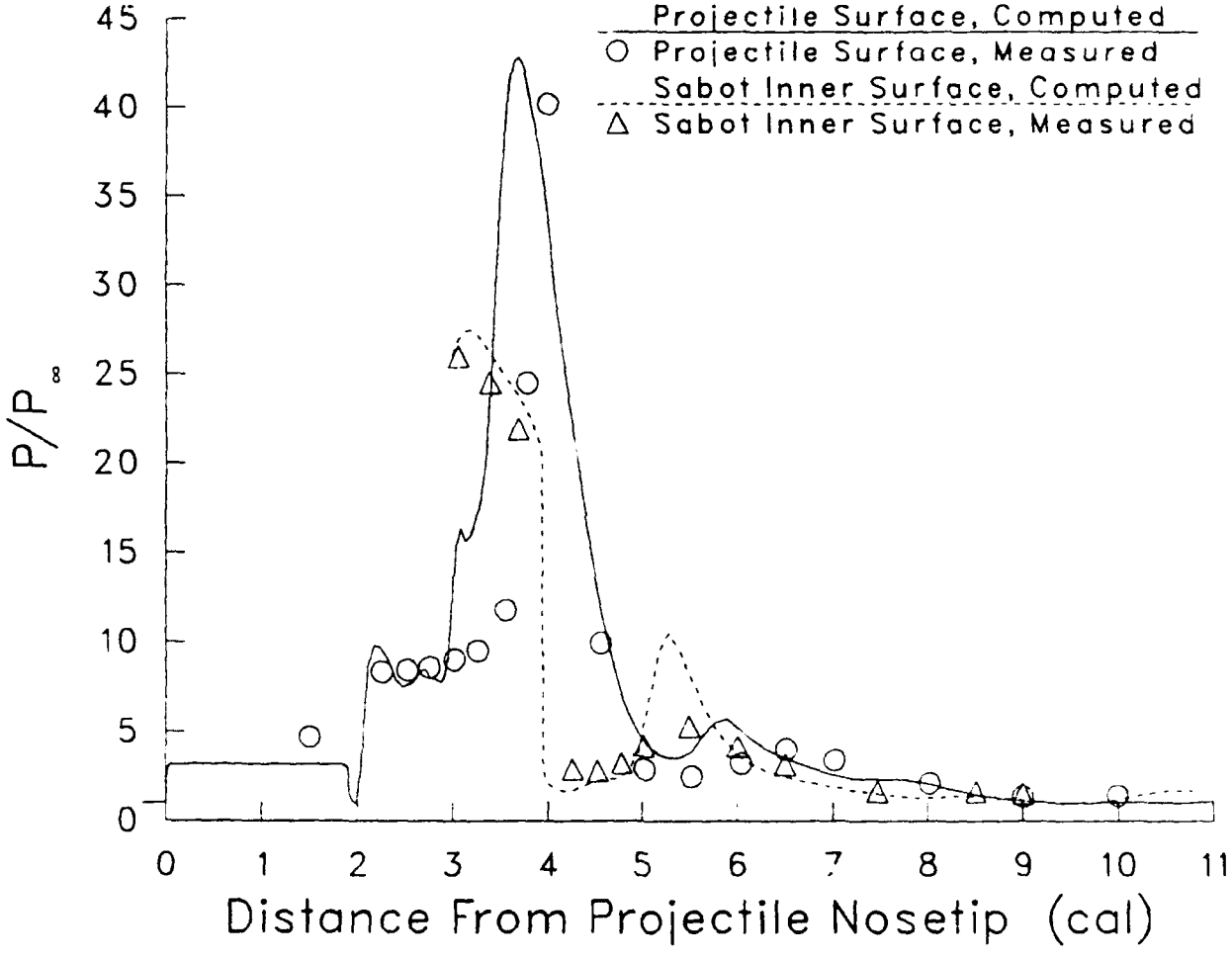

Figure 7. Laminar flow pressure distributions for projectile and sabot surfaces in the pitch plane ($\phi = 0, 180°$), $\Delta x/D = 0$, $\Delta y/D = .75$, $\alpha = 0°$.

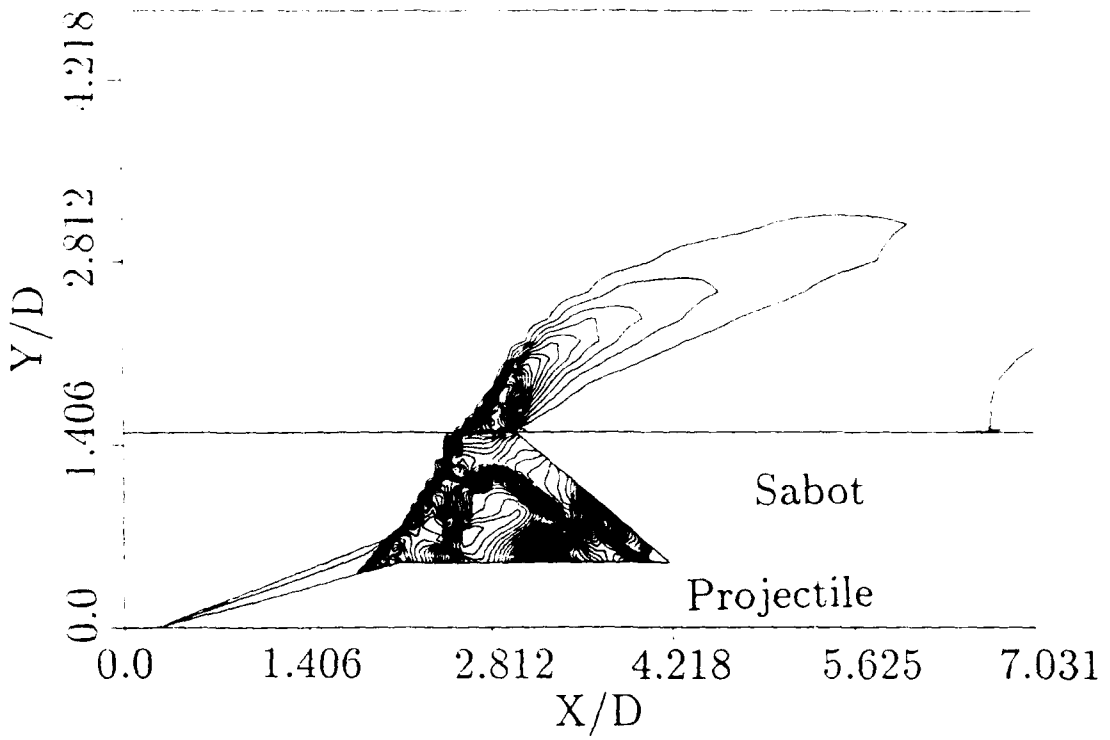

Figure 8. Laminar flow pressure contours in the pitch plane ($\sigma = 0, 180^{\circ}$) for $\triangle x/D = 0$, $\triangle y/D = 0.0$, $\alpha = 0^{\circ}$.

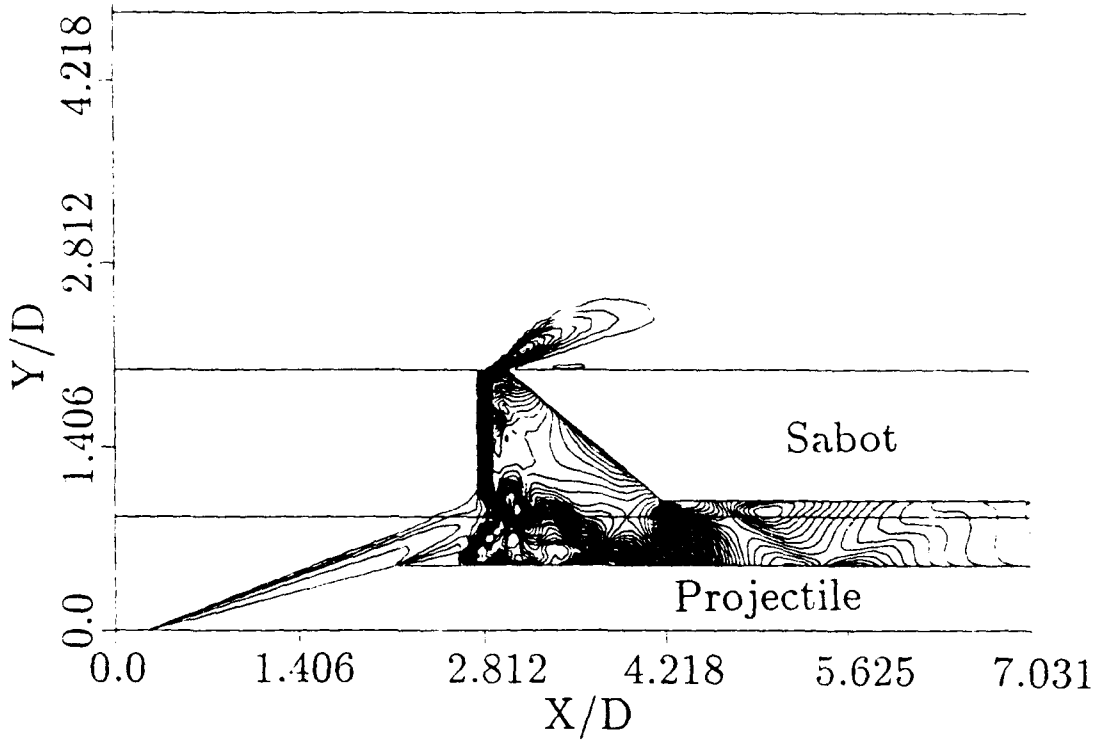

Figure 9. Laminar flow pressure contours in the pitch plane ($\sigma = 0, 180^{\circ}$) for $\triangle x/D = 0$, $\triangle y/D = 0.5$, $\alpha = 0^{\circ}$.

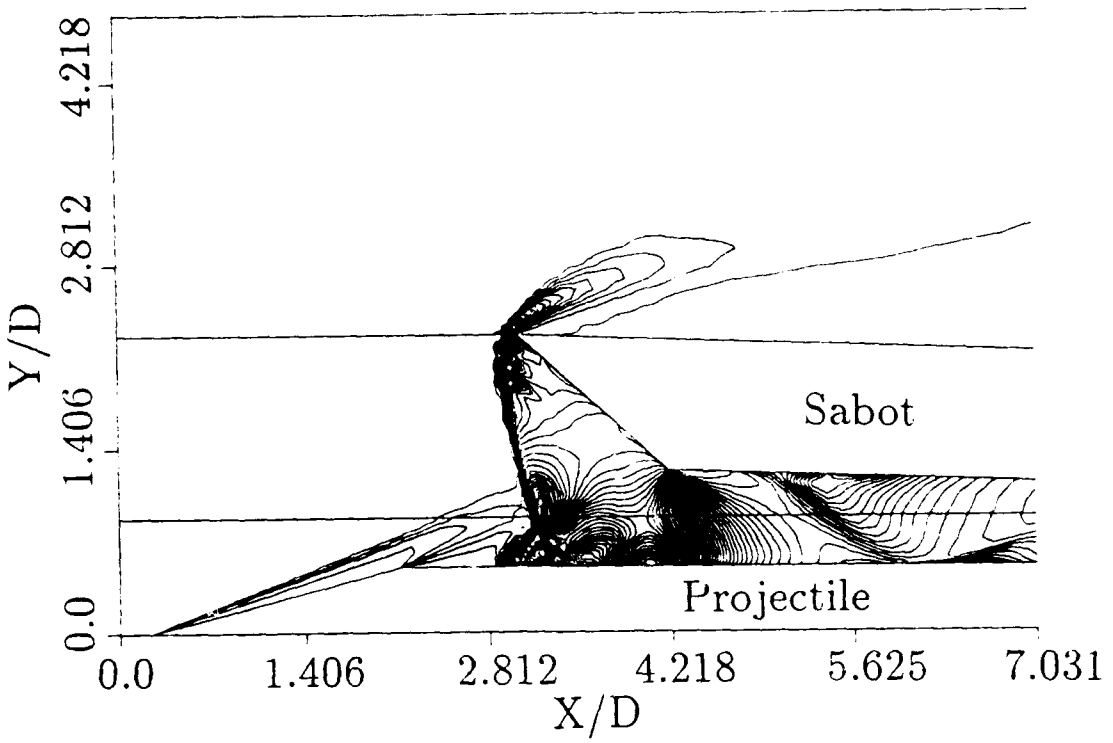

Figure 10. Laminar flow pressure contours in the pitch plane ($o = 0, 180°$) for $\triangle x/D = 0$, $\triangle y/D = 0.5$, $\alpha = 2°$.

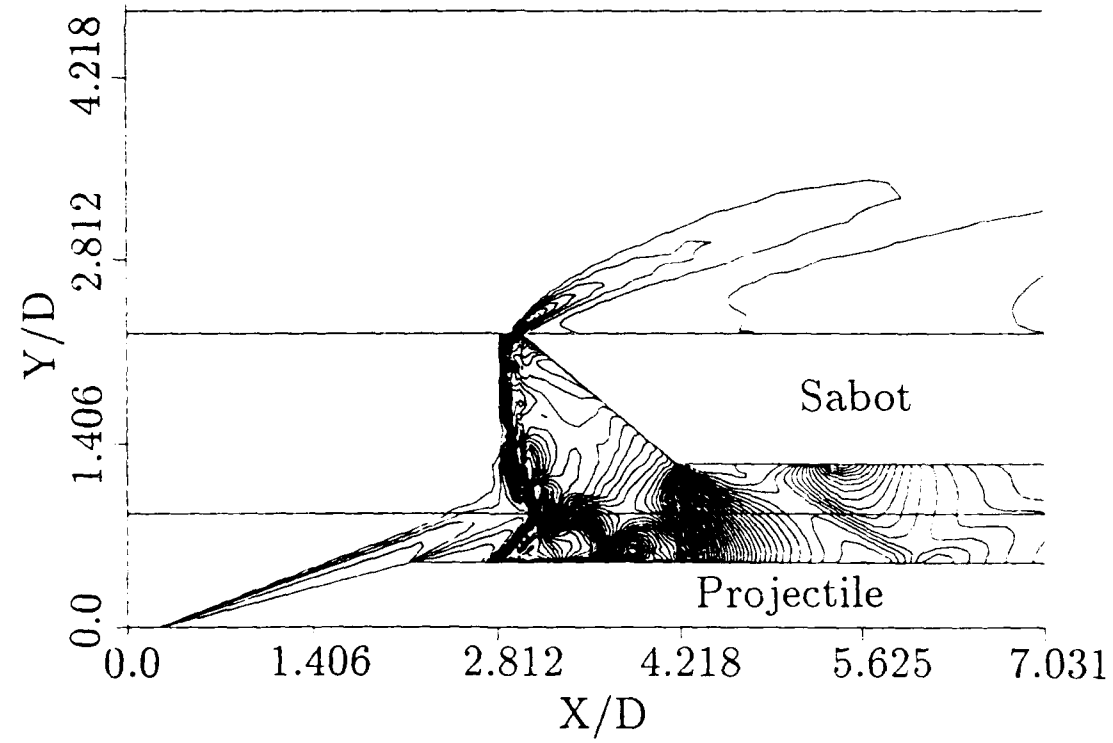

Figure 11. Laminar flow pressure contours in the pitch plane ($o = 0, 180°$) for $\triangle x/D = 0$, $\triangle y/D = 0.75$, $\alpha = 0°$.

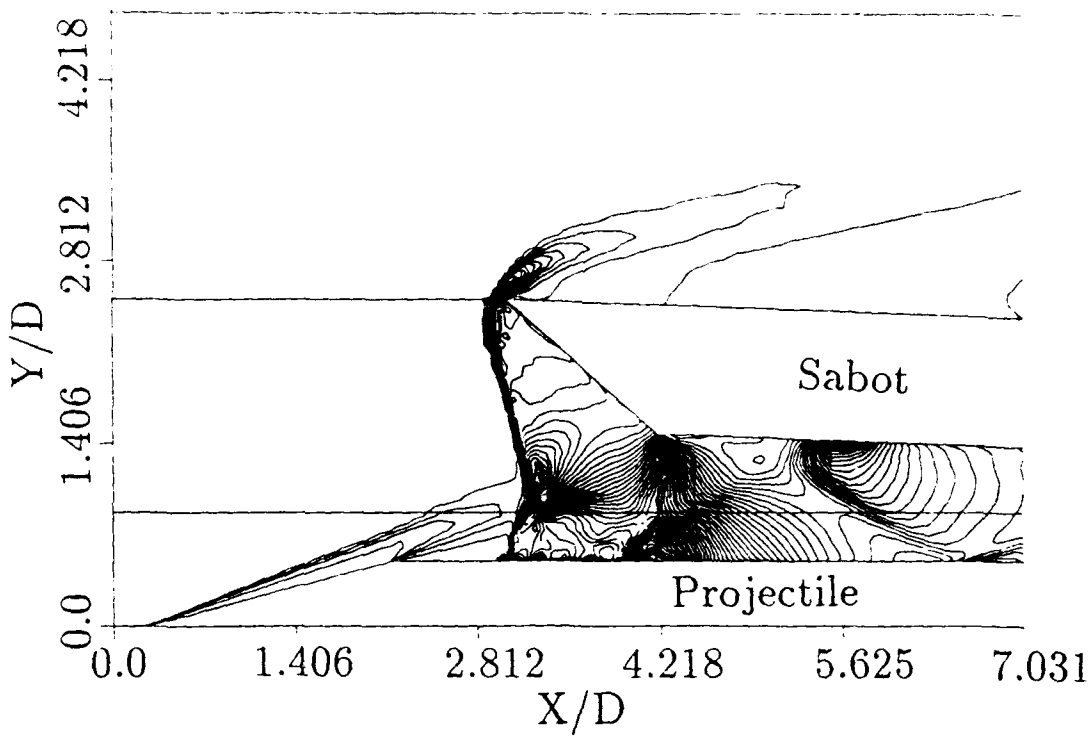

Figure 12. Laminar flow pressure contours in the pitch plane ($\phi = 0, 180°$) for $\Delta x/D = 0$, $\Delta y/D = 0.75$, $\alpha = 2°$.

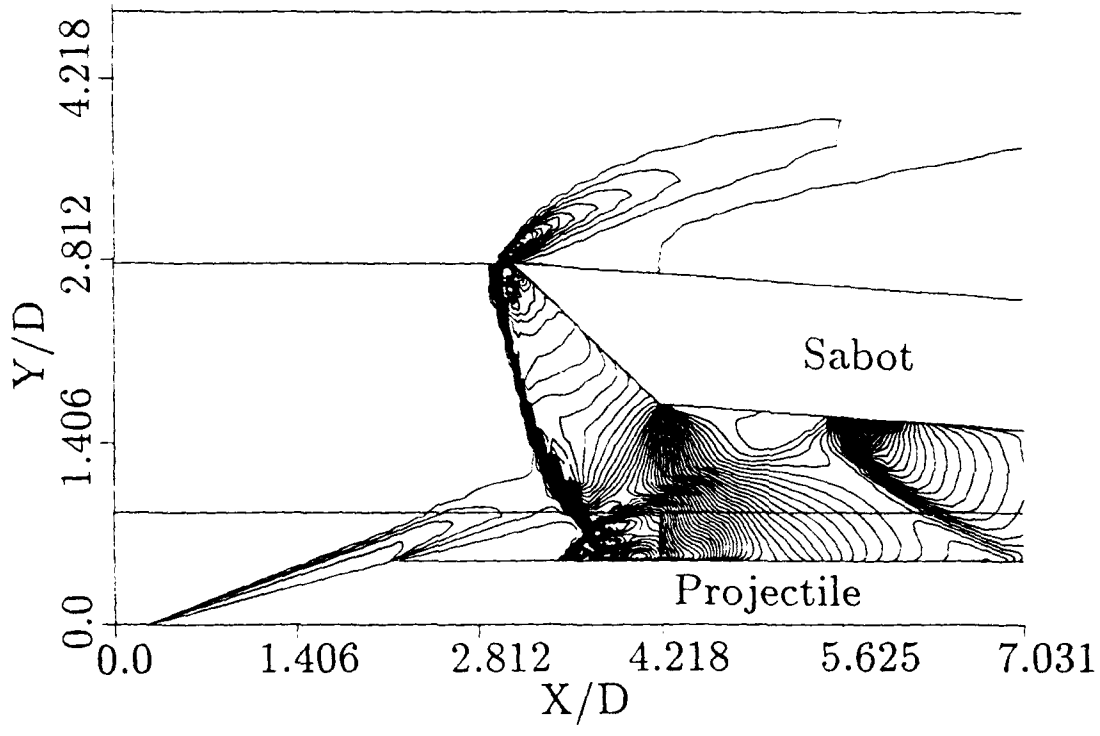

Figure 13. Laminar flow pressure contours in the pitch plane ($\phi = 0, 180°$) for $\Delta x/D = 0$, $\Delta y/D = 0.75$, $\alpha = 4°$.

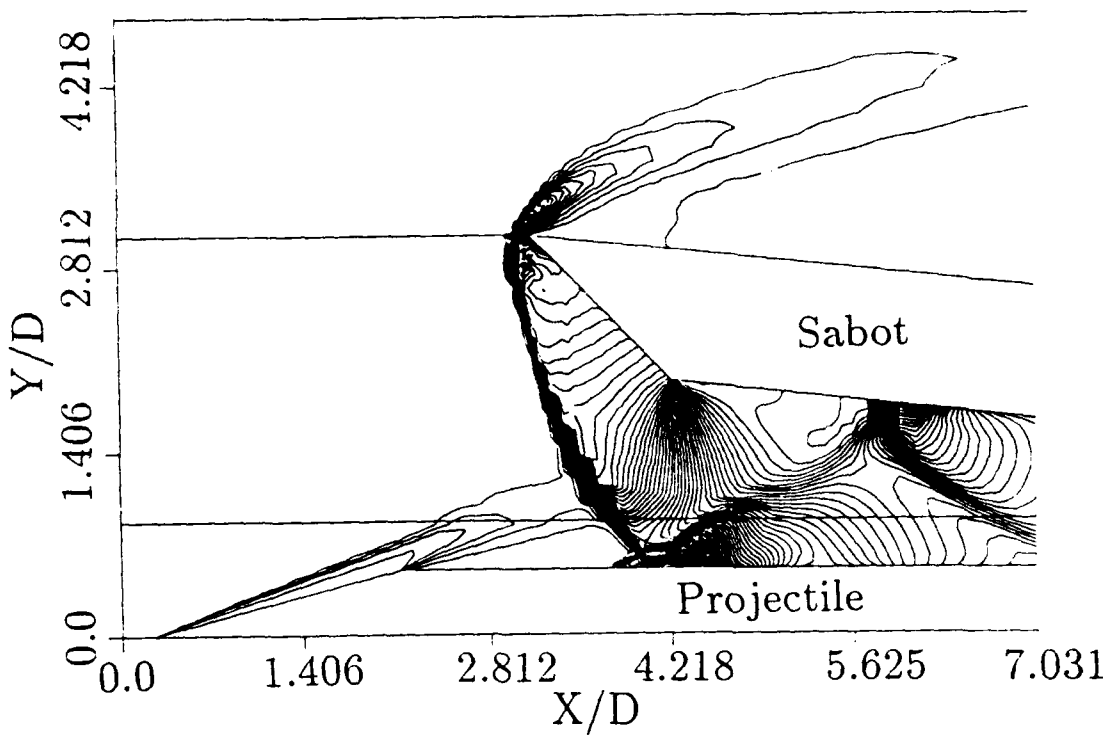

Figure 14. Laminar flow pressure contours in the pitch plane ($\phi = 0, 180°$) for $\triangle x/D = 0$, $\triangle y/D = 0.75$, $\alpha = 6°$.

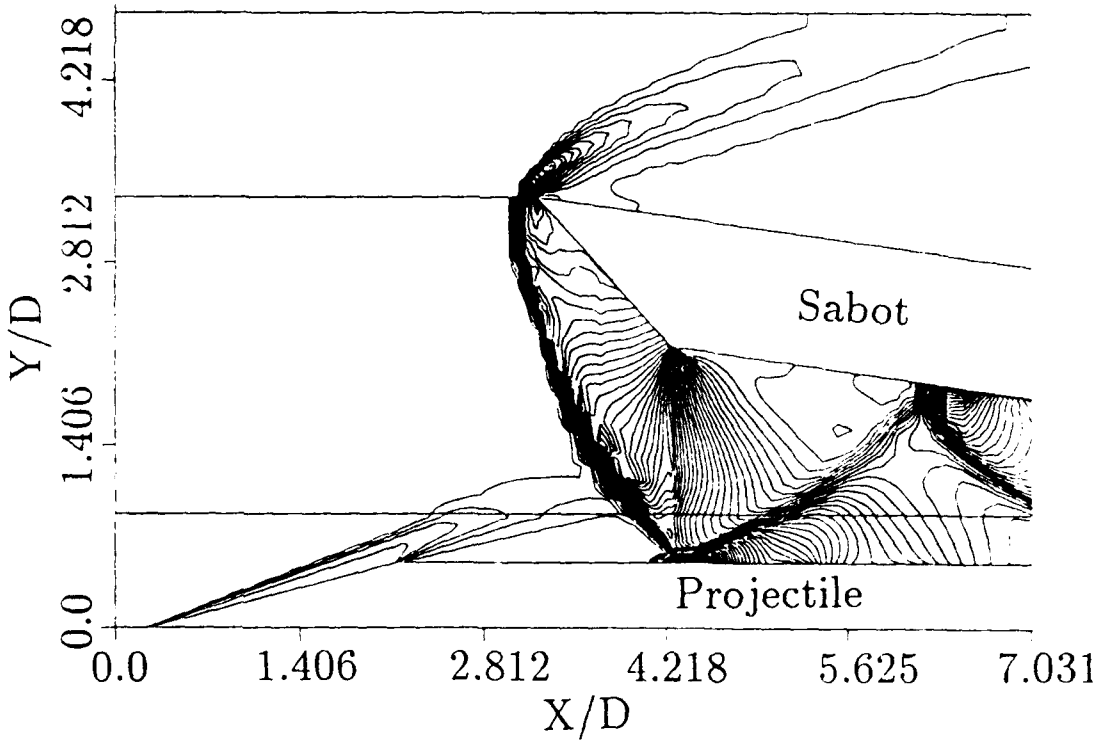

Figure 15. Laminar flow pressure contours in the pitch plane ($\phi = 0, 180°$) for $\triangle x/D = 0$, $\triangle y/D = 0.75$, $\alpha = 8°$.

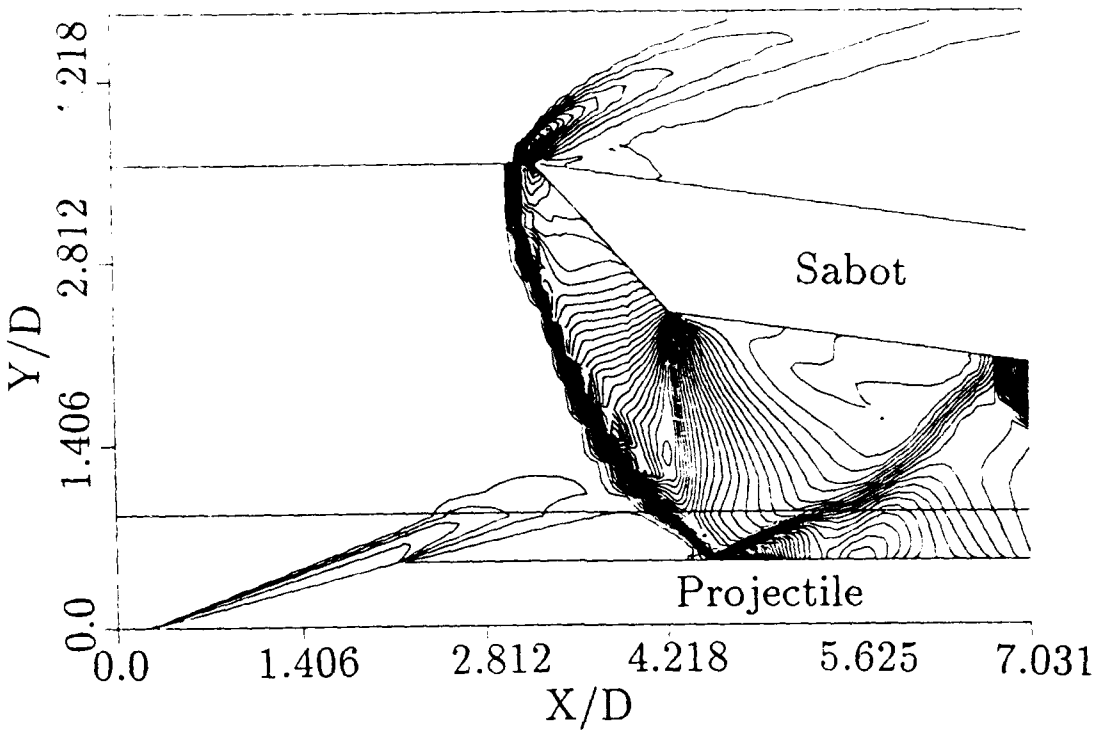

Figure 16. Laminar flow pressure contours in the pitch plane ($\phi = 0, 180°$) for $\Delta x/D = 0$, $\Delta y/D = 1.0$, $\alpha = 8°$.

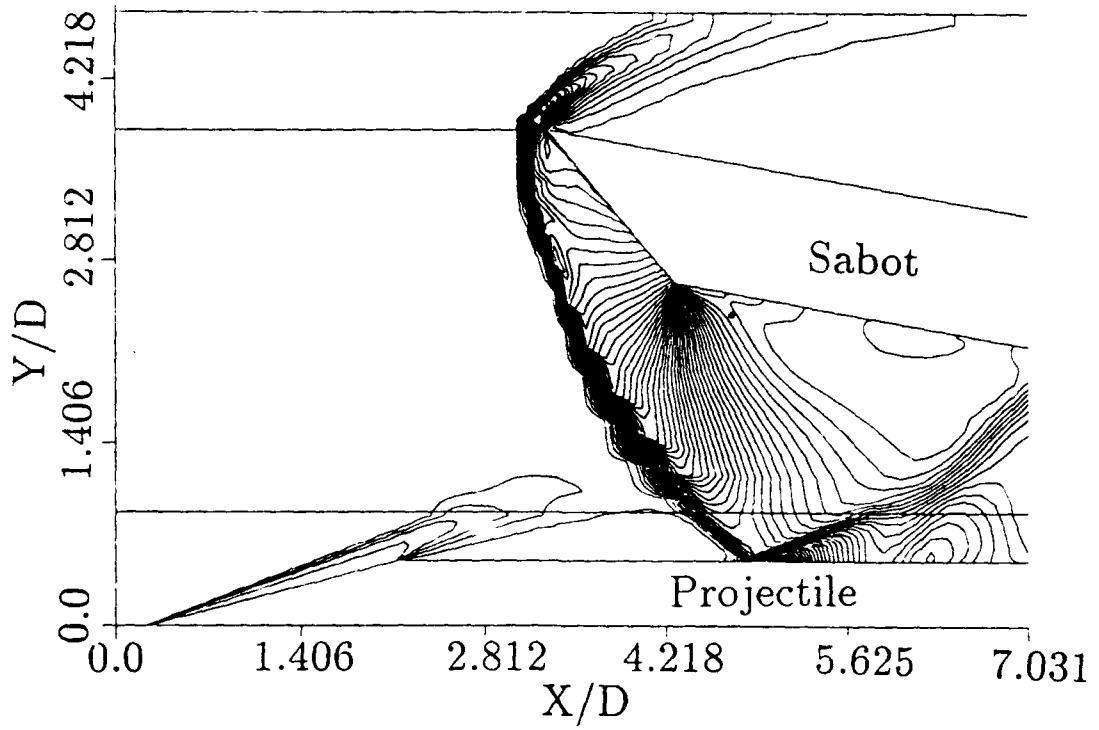

Figure 17. Laminar flow pressure contours in the pitch plane ($\phi = 0, 180°$) for $\Delta x/D = 0$, $\Delta y/D = 1.0$, $\alpha = 10°$.

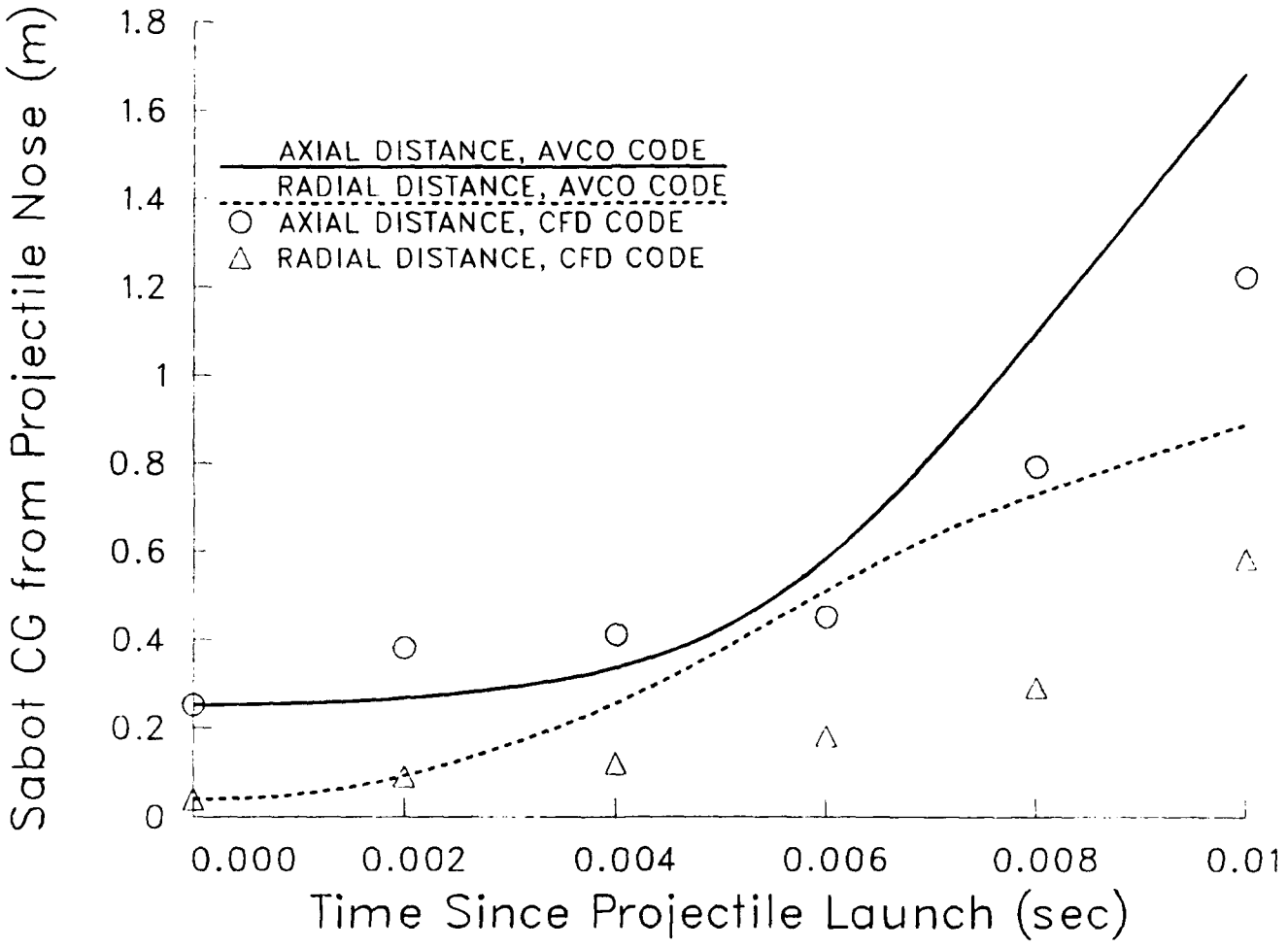

Figure 18. Trajectory of sabot center of mass computed using AVCO design code and present simulation using CFD.

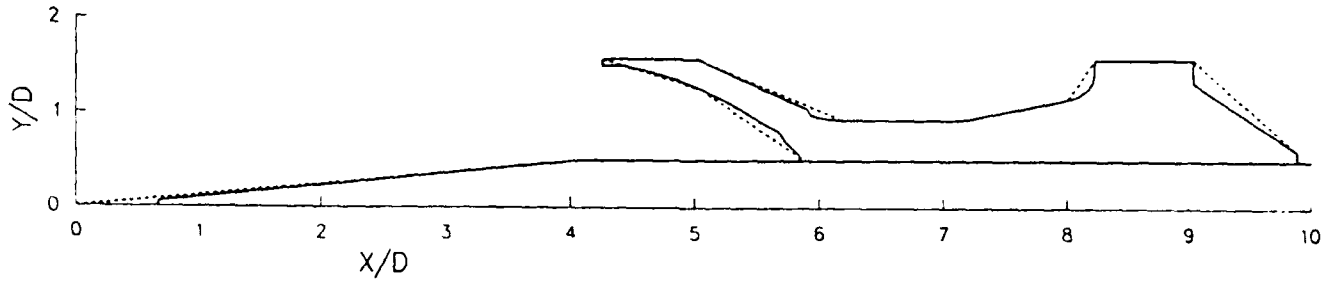

Figure 19. M865 projectile/sabot configuration. Solid line is actual geometry. Dashed line is computational geometry.

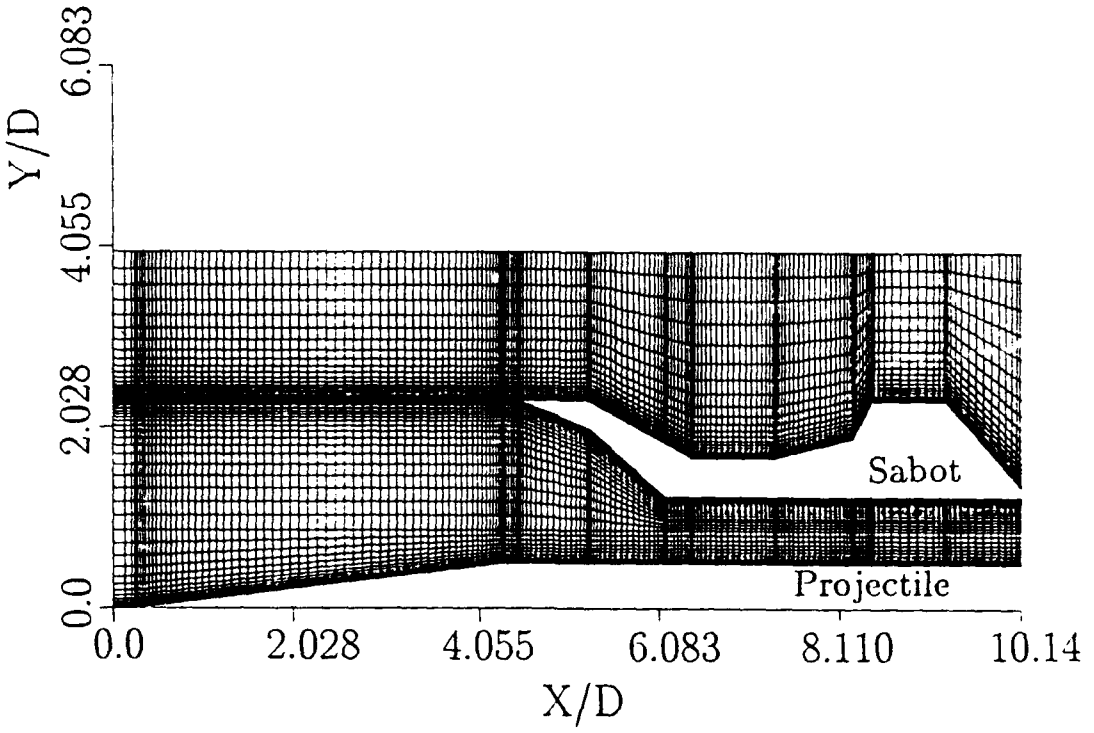

Figure 20. Structured grid (pitch plane view) for M829 projectile/sabot.

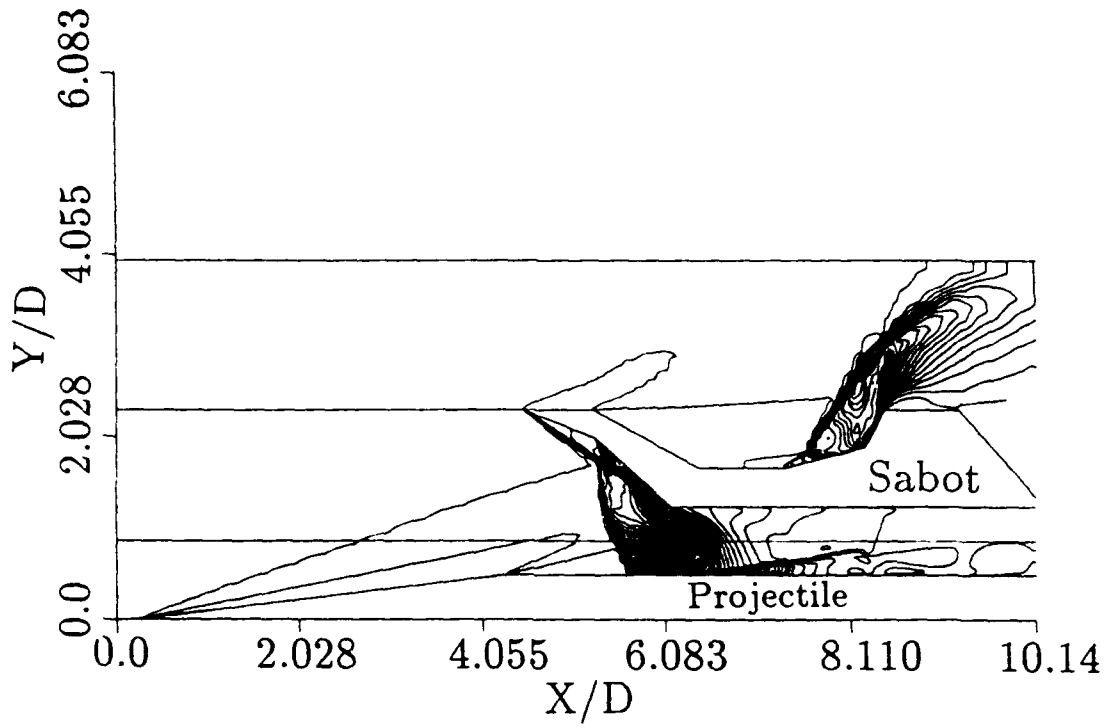

Figure 21. Laminar flow pressure contours in the pitch plane ($\phi = 0, 180°$) for M865 sabot, $\Delta x/D = .957$, $\Delta y/D = .75$, $\alpha = 0°$.

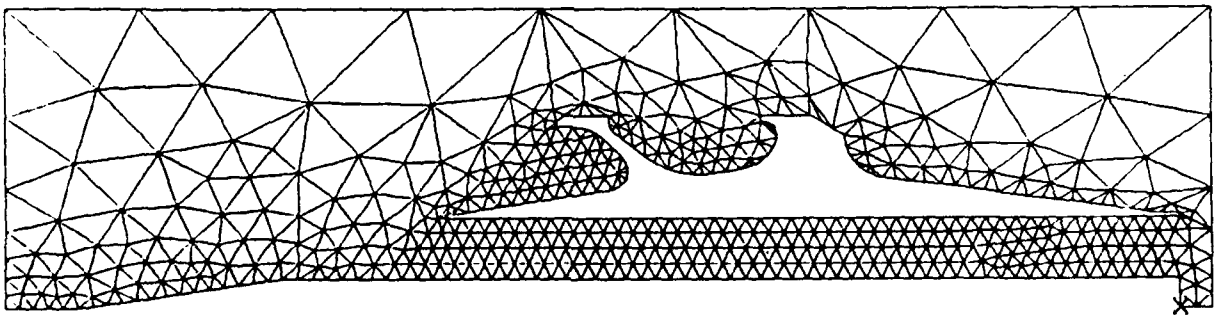

Figure 22. Unstructured grid (pitch plane view) for M829 projectile/sabot.

INTENTIONALLY LEFT BLANK

5. REFERENCES

Baldwin, B.S., and Lomax, H., "Thin Layer Approximation and Algebraic Model for Separated Turbulent Flows." AIAA-78-257, Proceedings of the 16th AIAA Aerospace Sciences Meeting, Huntsville AL, Jan. 1978.

Chakravarthy, S.R., Szema, K.Y., Goldberg, U.C., Gorski, J.J., and Osher, S., "Application of a New Class of High Accuracy TVD Schemes to the Navier-Stokes Equations," AIAA-85-0165, Proceedings of the 23rd AIAA Aerospace Sciences Meeting, Reno NV, Jan. 1985.

Chakravarthy, S.R., Szema, K.Y., and Haney, J.W., "Unified Nose to Tail Computational Method for Hypersonic Vehicle Applications," AIAA-88-2564, Proceedings of the 6th AIAA Applied Aerodynamics Conference, Williamsburg VA, June, 1988.

Chakravarthy, S.R., Szema, K.Y., and Chen, C.L., "A Universe Series Code for Inviscid CFD with Space Shuttle Applications Using Unstructured Grid," AIAA-91-3340, Proceedings of the 9th AIAA Applied Aerodynamics Conference, Baltimore MD, Sept. 1991.

Crimi, P., and Siegelman, D., "Analysis of Mechanical and Gasdynamic Loadings During Sabot Discard from Gun-Launched Projectiles," ARBRL-CR-341, US Army Ballistic Research Laboratory, Aberdeen Proving Ground, MD, June 1977.

Goldberg, U.C., "Separated Flow Treatment with a New Turbulence Model," AIAA Journal, Vol. 24, No. 10, Oct. 1986, pp. 1711-1713.

Mazor, G., Ben-Dor, G., and Igra, O., "A Simple and Accurate Expression for the Viscosity of Nonpolar Diatomic Gases up to 10,000 K," AIAA Journal, Vol. 23, No. 4, April 1985, pp. 636-638.

Nusca, M.J., "Computational Fluid Dynamics Application to the Aerodynamics of Symmetric Sabot Discard," AIAA-90-3096, Proceedings of the 8th AIAA Applied Aerodynamics Conference, Portland OR, August, 1990.

Nusca, M.J., "Computational Fluid Dynamics Application to the Aerodynamics of Symmetric Sabot Discard," Technical Report BRL-TR-3167, US Army Ballistic Research Laboratory, Aberdeen Proving Ground, MD, Oct. 1990.

Nusca, M.J., "Numerical Simulation of Sabot Discard Aerodynamics Using Computational Fluid Dynamics," Proceedings of 1991 Simulation Multiconference, Ballistics Simulation II, Society for Computer Simulation International, New Orleans, LA, April 1991.

Nusca, M.J., "Numerical Simulation of Sabot Discard Aerodynamics Using Computational Fluid Dynamics," Proceedings of 1991 Summer Computer Simulation Conference, Society for Computer Simulation International, Baltimore, MD, July 1991.

Schmidt, E.M. and Shear D.D., "Aerodynamic Interference During Sabot Discard," Journal of Spacecraft and Rockets, AIAA, Vol. 15, No. 3, May-June 1978, pp. 162-167.

Schmidt, E.M., "Wind-Tunnel Measurements of Sabot-Discard Aerodynamics," Journal of Spacecraft and Rockets, AIAA, Vol. 18, No. 3, May-June 1981, pp. 235-240.

Siegelman, D., Wang, J., and Crimi, P., "Computation of Sabot Discard," ARBRL-CR-505, US Army Ballistic Research Laboratory, Aberdeen Proving Ground, MD, Feb. 1983.

LIST OF SYMBOLS

cal	= caliber, D
c_p	= specific heat capacity, constant p
c_v	= specific heat capacity, constant volume
D	= diameter of projectile cylinder section
e	= specific total internal energy
F, G, H	= flux vectors (Eq. 1)
M	= Mach number
Pr	= Prandtl number
p	= pressure
$\dot{q}$	= heat transfer rate
$\Re$	= specific gas constant
T	= temperature
t	= time
U	= mean streamwise velocity
u, v, w	= cartesian velocity components
W	= dependent variable vector (Eq. 1)
x, y, z	= cartesian coordinates
$\triangle x$	= horizontal distance between projectile and sabot bases
$\triangle y$	= vertical distance between projectile and sabot surfaces

Greek Symbols

α	= sabot angle of attack wrt the projectile
γ	= ratio of specific heats, c_p/c_v
ζ	= transformed coordinate
η	= transformed coordinate
μ	= molecular viscosity
ξ	= transformed coordinate

ρ = density

σ_{xx}, σ_{yy}, σ_{zz} = normal stress tensors

τ = transformed time

τ_{xy}, τ_{xz}, τ_{yz} = shear stress tensors

ϕ = azimuthal angle, 0 and 180° for pitch plane, clockwise looking downstream

Subscripts

t = turbulence quantity

x, y, z = denotes spacial components

ζ = ζ-direction transform coefficient

η = η-direction transform coefficient

ξ = ξ-direction transform coefficient

∞ = freestream quantity

No. of Copies	Organization
2	Administrator Defense Technical Info Center ATTN: DTIC-DDA Cameron Station Alexandria, VA 22304-6145
1	Commander U.S. Army Materiel Command ATTN: AMCAM 5001 Eisenhower Ave. Alexandria, VA 22333-0001
1	Director U.S. Army Research Laboratory ATTN: AMSRL-OP-CI-AD, Tech Publishing 2800 Powder Mill Rd. Adelphi, MD 20783-1145
1	Director U.S. Army Research Laboratory ATTN: AMSRL-OP-CI-AD, Records Management 2800 Powder Mill Rd. Adelphi, MD 20783-1145
2	Commander U.S. Army Armament Research, Development, and Engineering Center ATTN: SMCAR-IMI-I Picatinny Arsenal, NJ 07806-5000
2	Commander U.S. Army Armament Research, Development, and Engineering Center ATTN: SMCAR-TDC Picatinny Arsenal, NJ 07806-5000
1	Director Benet Weapons Laboratory U.S. Army Armament Research, Development, and Engineering Center ATTN: SMCAR-CCB-TL Watervliet, NY 12189-4050
1	Director U.S. Army Advanced Systems Research and Analysis Office (ATCOM) ATTN: AMSAT-R-NR, M/S 219-1 Ames Research Center Moffett Field, CA 94035-1000

No. of Copies	Organization
1	Commander U.S. Army Missile Command ATTN: AMSMI-RD-CS-R (DOC) Redstone Arsenal, AL 35898-5010
1	Commander U.S. Army Tank-Automotive Command ATTN: AMSTA-JSK (Armor Eng. Br.) Warren, MI 48397-5000
1	Director U.S. Army TRADOC Analysis Command ATTN: ATRC-WSR White Sands Missile Range, NM 88002-5502
(Class. only) 1	Commandant U.S. Army Infantry School ATTN: ATSH-CD (Security Mgr.) Fort Benning, GA 31905-5660
(Unclass. only) 1	Commandant U.S. Army Infantry School ATTN: ATSH-WCB-O Fort Benning, GA 31905-5000
1	WL/MNOI Eglin AFB, FL 32542-5000
	Aberdeen Proving Ground
2	Dir, USAMSAA ATTN: AMXSY-D AMXSY-MP, H. Cohen
1	Cdr, USATECOM ATTN: AMSTE-TC
1	Dir, ERDEC ATTN: SCBRD-RT
1	Cdr, CBDA ATTN: AMSCB-CII
1	Dir, USARL ATTN: AMSRL-SL-I
10	Dir, USARL ATTN: AMSRL-OP-CI-B (Tech Lib)

No. of Copies	Organization
1	Chairman DOD Explosives Safety Board Room 856-C Hoffman Bldg. I 2461 Eisenhower Avenue Alexandria, VA 22331-0600
1	Headquarters U.S. Army Materiel Command ATTN: AMCICP-AD, M. Fisette 5001 Eisenhower Ave. Alexandria, VA 22333-0001
1	U.S. Army Ballistic Missile Defense Systems Command Advanced Technology Center P.O. Box 1500 Huntsville, AL 35807-3801
1	Department of the Army Office of the Product Manager 155mm Howitzer, M109A6, Paladin ATTN: SFAE-AR-HIP-IP, Mr. R. De Kleine Picatinny Arsenal, NJ 07806-5000
3	Project Manager Advanced Field Artillery System ATTN: SFAE-ASM-AF-E, LTC A. Ellis T. Kuriata J. Shields Picatinny Arsenal, NJ 07801-5000
1	Project Manager Advanced Field Artillery System ATTN: SFAE-ASM-AF-Q, W. Warren Picatinny Arsenal, NJ 07801-5000
2	Commander Production Base Modernization Agency U.S. Army Armament Research, Development, and Engineering Center ATTN: AMSMC-PBM, A. Siklosi AMSMC-PBM-E, L. Laibson Picatinny Arsenal, NJ 07806-5000
4	PEO-Armaments Project Manager Tank Main Armament System ATTN: AMCPM-TMA AMCPM-TMA-105 AMCPM-TMA-120 AMCPM-TMA-AS, H. Yuen Picatinny Arsenal, NJ 07806-5000
4	Commander U.S. Army Armament Research, Development, and Engineering Center ATTN: SMCAR-CCH-V, C. Mandala E. Fennell SMCAR-CCH-T, L. Rosendorf SMCAR-CCS Picatinny Arsenal, NJ 07806-5000
19	Commander U.S. Army Armament Research, Development, and Engineering Center ATTN: SMCAR-AEE, J. Lannon SMCAR-AEE-B, A. Beardell D. Downs S. Einstein S. Westley S. Bernstein J. Rutkowski B. Brodman P. O'Reilly R. Cirincione A. Grabowsky P. Hui J. O'Reilly SMCAR-AFE-WW, M. Mezger J. Pinto D. Wiegand P. Lu C. Hu SMCAR-AES, S. Kaplowitz Picatinny Arsenal, NJ 07806-5000
1	Commander U.S. Army Armament Research, Development and Engineering Center ATTN: SMCAR-HFM, E. Barrieres Picatinny Arsenal, NJ 07806-5000

No. of Copies	Organization
9	Commander U.S. Army Armament Research, Development and Engineering Center ATTN: SMCAR-FSA-F, LTC R. Riddle SMCAR-FSC, G. Ferdinand SMCAR-FS, T. Gora SMCAR-FS-DH, J. Feneck SMCAR-FSS-A, R. Kopmann B. Machek L. Pinder SMCAR-FSN-N, K. Chung Picatinny Arsenal, NJ 07806-5000
3	Director Benet Weapons Laboratories ATTN: SMCAR-CCB-RA, G.P. O'Hara G.A. Pflegl SMCAR-CCB-S, F. Heiser Watervliet, NY 12189-4050
2	Commander U.S. Army Research Office ATTN: Technical Library D. Mann P.O. Box 12211 Research Triangle Park, NC 27709-2211
1	Director Army Research Office ATTN: AMXRO-MCS, Mr. K. Clark P.O. Box 12211 Research Triangle Park, NC 27709-2211
1	Director Army Research Office ATTN: AMXRO-RT-IP, Library Services P.O. Box 12211 Research Triangle Park, NC 27709-2211
1	Commander, USACECOM R&D Technical Library ATTN: ASQNC-ELC-IS-L-R, Myer Center Fort Monmouth, NJ 07703-5301
1	Commandant U.S. Army Aviation School ATTN: Aviation Agency Fort Rucker, AL 36360

No. of Copies	Organization
1	Program Manager U.S. Tank-Automotive Command ATTN: AMCPM-ABMS, T. Dean Warren, MI 48092-2498
1	Project Manager U.S. Tank-Automotive Command Fighting Vehicle Systems ATTN: SFAE-ASM-BV Warren, MI 48397-5000
1	Project Manager, Abrams Tank System ATTN: SFAE-ASM-AB Warren, MI 48397-5000
1	Director HQ, TRAC RPD ATTN: ATCD-MA Fort Monroe, VA 23651-5143
1	Commander U.S. Army Belvoir Research and Development Center ATTN: STRBE-WC Fort Belvoir, VA 22060-5006
1	Director U.S. Army TRAC-Ft. Lee ATTN: ATRC-L, Mr. Cameron Fort Lee, VA 23801-6140
1	Commandant U.S. Army Command and General Staff College Fort Leavenworth, KS 66027
1	Commandant U.S. Army Special Warfare School ATTN: Rev and Trng Lit Div Fort Bragg, NC 28307
1	Commander Radford Army Ammunition Plant ATTN: SMCAR-QA/HI LIB Radford, VA 24141-0298

No. of Copies	Organization
1	Commander U.S. Army Foreign Science and Technology Center ATTN: AMXST-MC-3 220 Seventh Street, NE Charlottesville, VA 22901-5396
2	Commandant U.S. Army Field Artillery Center and School ATTN: ATSF-CO-MW, E. Dublisky ATSF-CN, P. Gross Ft. Sill, OK 73503-5600
1	Commandant U.S. Army Armor School ATTN: ATZK-CD-MS, M. Falkovitch Armor Agency Fort Knox, KY 40121-5215
2	Commander Naval Sea Systems Command ATTN: SEA 62R SEA 64 Washington, DC 20362-5101
1	Commander Naval Air Systems Command ATTN: AIR-954-Tech Library Washington, DC 20360
4	Commander Naval Research Laboratory ATTN: Technical Library Code 4410, K. Kailasanate J. Boris E. Oran Washington, DC 20375-5000
1	Office of Naval Research ATTN: Code 473, R.S. Miller 800 N. Quincy Street Arlington, VA 22217-9999

No. of Copies	Organization
1	Office of Naval Technology ATTN: ONT-213, D. Siegel 800 N. Quincy St. Arlington, VA 22217-5000
2	Commander Naval Surface Warfare Center ATTN: Code 730 Code R-13, R. Bernecker Silver Spring, MD 20903-5000
7	Commander Naval Surface Warfare Center ATTN: T.C. Smith K. Rice S. Mitchell S. Peters J. Consaga C. Gotzmer Technical Library Indian Head, MD 20640-5000
4	Commander Naval Surface Warfare Center ATTN: Code G30, Guns & Munitions Div Code G32, Guns Systems Div Code G33, T. Doran Code E23 Technical Library Dahlgren, VA 22448-5000
5	Commander Naval Air Warfare Center ATTN: Code 388, C.F. Price T. Boggs Code 3895, T. Parr R. Derr Information Science Division China Lake, CA 93555-6001
1	Commanding Officer Naval Underwater Systems Center ATTN: Code 5B331, Technical Library Newport, RI 02840
1	AFOSR/NA ATTN: J. Tishkoff Bolling AFB, D.C. 20332-6448

No. of Copies	Organization
1	OLAC PL/TSTL ATTN: D. Shiplett Edwards AFB, CA 93523-5000
3	AL/LSCF ATTN: J. Levine T. Quinn T. Edwards Edwards AFB, CA 93523-5000
1	WL/MNAA ATTN: B. Simpson Eglin AFB, FL 32542-5434
1	WL/MNME Energetic Materials Branch 2306 Perimeter Rd, STE 9 Eglin AFB, FL 32542-5910
1	WL/MNSH ATTN: R. Drabczuk Eglin AFB, FL 32542-5434
2	NASA Langley Research Center ATTN: M.S. 408, W. Scallion D. Witcofski Hampton, VA 23605
1	Central Intelligence Agency Office of the Central References Dissemination Branch Room GE-47, HQS Washington, DC 20502
1	Central Intelligence Agency ATTN: J. Backofen NHB, Room 5N01 Washington, DC 20505
1	SDIO/TNI ATTN: L.H. Caveny Pentagon Washington, DC 20301-7100
1	SDIO/DA ATTN: E. Gerry Pentagon Washington, DC 21301-7100

No. of Copies	Organization
2	HQ DNA ATTN: D. Lewis A. Fahey 6801 Telegraph Rd. Alexandria, VA 22310-3398
1	Director Sandia National Laboratories Energetic Materials & Fluid Mechanics Department, 1512 ATTN: M. Baer P.O. Box 5800 Albuquerque, NM 87185
1	Director Sandia National Laboratories Combustion Research Facility ATTN: R. Carling Livermore, CA 94551-0469
1	Director Sandia National Laboratories ATTN: 8741, G. A. Beneditti P.O. Box 969 Livermore, CA 94551-0969
2	Director Lawrence Livermore National Laboratory ATTN: L-355, A. Buckingham M. Finger P.O. Box 808 Livermore, CA 94550-0622
2	Director Los Alamos Scientific Lab ATTN: T3/D. Butler M. Division/B. Craig P.O. Box 1663 Los Alamos, NM 87544
2	Battelle ATTN: TACTEC Library, J.N. Huggins V. Levin 505 King Avenue Columbus, OH 43201-2693
1	Battelle PNL ATTN: M.C.C. Bampton P.O. Box 999 Richland, WA 99352

No. of Copies	Organization
1	Institute of Gas Technology ATTN: D. Gidaspow 3424 S. State Street Chicago, IL 60616-3896
1	Institute for Advanced Technology ATTN: T.M. Kiehne The University of Texas of Austin 4030-2 W. Braker Lane Austin, TX 78759-5329
2	CPIA - JHU ATTN: H. J. Hoffman T. Christian 10630 Little Patuxent Parkway Suite 202 Columbia, MD 21044-3200
1	Brigham Young University Department of Chemical Engineering ATTN: M. Beckstead Provo, UT 84601
1	Jet Propulsion Laboratory California Institute of Technology ATTN: L.D. Strand, MS 125/224 4800 Oak Grove Drive Pasadena, CA 91109
1	California Institute of Technology 204 Karman Lab Main Stop 301-46 ATTN: F.E.C. Culick 1201 E. California Street Pasadena, CA 91109
3	Georgia Institute of Technology School of Aerospace Engineering ATTN: B.T. Zim E. Price W.C. Strahle Atlanta, GA 30332
1	Massachusetts Institute of Technology Department of Mechanical Engineering ATTN: T. Toong 77 Massachusetts Avenue Cambridge, MA 02139-4307
2	University of Illinois Department of Mechanical/Industry Engineering ATTN: H. Krier R. Beddini 144 MEB; 1206 N. Green St. Urbana, IL 61801-2978
1	University of Maryland ATTN: Dr. J.D. Anderson College Park, MD 20740
1	University of Massachusetts Department of Mechanical Engineering ATTN: K. Jakus Amherst, MA 01002-0014
1	University of Minnesota Department of Mechanical Engineering ATTN: E. Fletcher Minneapolis, MN 55414-3368
3	Pennsylvania State University Department of Mechanical Engineering ATTN: V. Yang K. Kuo C. Merkle University Park, PA 16802-7501
1	Rensselaer Polytechnic Institute Department of Mathematics Troy, NY 12181
1	Stevens Institute of Technology Davidson Laboratory ATTN: R. McAlevy III Castle Point Station Hoboken, NJ 07030-5907
1	Rutgers University Department of Mechanical and Aerospace Engineering ATTN: S. Temkin University Heights Campus New Brunswick, NJ 08903
1	University of Southern California Mechanical Engineering Department ATTN: OHE200, M. Gerstein Los Angeles, CA 90089-5199

No. of Copies	Organization
1	University of Utah Department of Chemical Engineering ATTN: A. Baer Salt Lake City, UT 84112-1194
1	Washington State University Department of Mechanical Engineering ATTN: C.T. Crowe Pullman, WA 99163-5201
1	AFELM, The Rand Corporation ATTN: Library D 1700 Main Street Santa Monica, CA 90401-3297
1	Arrow Technology Associates, Inc. ATTN: W. Hathaway P.O. Box 4218 South Burlington, VT 05401-0042
3	AAI Corporation ATTN: J. Hebert J. Frankle D. Cleveland P.O. Box 126 Hunt Valley, MD 21030-0126
2	Alliant Techsystems, Inc. ATTN: R.E. Tompkins J. Kennedy 7225 Northland Dr. Brooklyn Park, MN 55428
1	AVCO Everett Research Laboratory ATTN: D. Stickler 2385 Revere Beach Parkway Everett, MA 02149-5936
1	General Applied Sciences Lab ATTN: J. Erdos 77 Raynor Ave. Ronkonkama, NY 11779-6649
1	General Electric Company Tactical System Department ATTN: J. Mandzy 100 Plastics Ave. Pittsfield, MA 01201-3698
1	IITRI ATTN: M.J. Klein 10 W. 35th Street Chicago, IL 60616-3799

No. of Copies	Organization
4	Hercules, Inc. Radford Army Ammunition Plant ATTN: L. Gizzi D.A. Worrell W.J. Worrell C. Chandler Radford, VA 24141-0299
2	Hercules, Inc. Allegheny Ballistics Laboratory ATTN: William B. Walkup Thomas F. Farabaugh P.O. Box 210 Rocket Center, WV 26726
1	Hercules, Inc. Aerospace ATTN: R. Cartwright 100 Howard Blvd. Kenville, NJ 07847
1	Hercules, Inc. Hercules Plaza ATTN: B.M. Riggleman Wilmington, DE 19894
1	MBR Research Inc. ATTN: Dr. Moshe Ben-Reuven 601 Ewing St., Suite C-22 Princeton, NJ 08540
1	Olin Corporation Badger Army Ammunition Plant ATTN: F.E. Wolf Baraboo, WI 53913
3	Olin Ordnance ATTN: E.J. Kirschke A.F. Gonzalez D.W. Worthington P.O. Box 222 St. Marks, FL 32355-0222
1	Olin Ordnance ATTN: H.A. McElroy 10101 9th Street, North St. Petersburg, FL 33716
1	Paul Gough Associates, Inc. ATTN: P.S. Gough 1048 South St. Portsmouth, NH 03801-5423

No. of Copies	Organization
1	Physics International Library ATTN: H. Wayne Wampler P.O. Box 5010 San Leandro, CA 94577-0599
2	Princeton Combustion Research Laboratories, Inc. ATTN: N. Mer N.A. Messina Princeton Corporate Plaza 11 Deerpark Dr., Bldg IV, Suite 119 Monmouth Junction, NJ 08852
3	Rockwell International Rocketdyne Division ATTN: BA08, J. Flanagan J. Gray R.B. Edelman 6633 Canoga Avenue Canoga Park, CA 91303-2703
2	Rockwell International Science Center ATTN: Dr. S. Chakravarthy Dr. S. Palaniswamy 1049 Camino Dos Rios P.O. Box 1085 Thousand Oaks, CA 91360
1	Science Applications International Corp. ATTN: M. Palmer 2109 Air Park Rd. Albuquerque, NM 87106
1	Southwest Research Institute ATTN: J.P. Riegel 6220 Culebra Road P.O. Drawer 28510 San Antonio, TX 78228-0510
1	Sverdrup Technology, Inc. ATTN: Dr. John Deur 2001 Aerospace Parkway Brook Park, OH 44142
3	Thiokol Corporation Elkton Division ATTN: R. Willer R. Biddle Tech Library P.O. Box 241 Elkton, MD 21921-0241
1	Veritay Technology, Inc. ATTN: E. Fisher 4845 Millersport Hwy. East Amherst, NY 14501-0305
1	Universal Propulsion Company ATTN: H.J. McSpadden 25401 North Central Ave. Phoenix, AZ 85027-7837
1	SRI International Propulsion Sciences Division ATTN: Tech Library 333 Ravenwood Avenue Menlo Park, CA 94025-3493
	Aberdeen Proving Ground
1	Cdr, USACSTA ATTN: STECS-PO/R. Hendricksen

USER EVALUATION SHEET/CHANGE OF ADDRESS

This Laboratory undertakes a continuing effort to improve the quality of the reports it publishes. Your comments/answers to the items/questions below will aid us in our efforts.

1. ARL Report Number ARL-TR-204 Date of Report September 1993

2. Date Report Received _____

3. Does this report satisfy a need? (Comment on purpose, related project, or other area of interest for which the report will be used.) _____

4. Specifically, how is the report being used? (Information source, design data, procedure, source of ideas, etc.) _____

5. Has the information in this report led to any quantitative savings as far as man-hours or dollars saved, operating costs avoided, or efficiencies achieved, etc? If so, please elaborate. _____

6. General Comments. What do you think should be changed to improve future reports? (Indicate changes to organization, technical content, format, etc.) _____

CURRENT ADDRESS

_____
Organization

_____
Name

_____
Street or P.O. Box No.

_____
City, State, Zip Code

7. If indicating a Change of Address or Address Correction, please provide the Current or Correct address above and the Old or Incorrect address below.

OLD ADDRESS

_____
Organization

_____
Name

_____
Street or P.O. Box No.

_____
City, State, Zip Code

(Remove this sheet, fold as indicated, tape closed, and mail.)

(DO NOT STAPLE)

DEPARTMENT OF THE ARMY

OFFICIAL BUSINESS

BUSINESS REPLY MAIL
FIRST CLASS PERMIT No 0001, APG, MD

Postage will be paid by addressee

NO POSTAGE
NECESSARY
IF MAILED
IN THE
UNITED STATES

Director
U.S. Army Research Laboratory
ATTN: AMSRL-OP-CI-B (Tech Lib)
Aberdeen Proving Ground, MD 21005-5066